GRADED INFILL STRUCTURE OF WIND TURBINE BLADE ACCOUNTING FOR INTERNAL STRESS IN BIG AREA ADDITIVE MANUFACTURING

Seokpum Kim[1], Gregory Dreifus[2], Bentley Beard[1], Andrew Glick[3], Andrew Messing[1], Ahmed Arabi Hassen[1], John Lindahl[1], Peng Liu[1], Tyler Smith[1], Jordan Failla[1], Brian Post[1], John C. Bowers[4], Kenneth Stephenson[5], Lonnie Love[1], Vlastimil Kunc[1,6]

[1]Manufacturing Demonstration Facility, Oak Ridge National Laboratory, Oak Ridge, TN, 37831
[2]Department of Mechanical Engineering, Massachusetts Institute of Technology, Cambridge, MA 02139
[3]XZERES Corp., Wilsonville, OR 97070
[4]Department of Computer Science, James Madison University, Harrisonburg, VA 22807
[5]Department of Mathematics, University of Tennessee Knoxville, Knoxville, TN 37996
[6]School of Materials Engineering, Purdue University, West Lafayette, IN 47907

ABSTRACT

In additively manufactured (AM) components, infill structure significantly affects the mechanical performance of the final printed part. However, mechanical stress induced by operation loads has been so far neglected for infill patterning. Most slicers currently available in the market provide infill patterns that are uniform in shape and size regardless of the operational loading. We develop a design approach for infill patterns that accounts for the induced stress. This approach differs from topology optimization as it focuses on the porous infill, which allows the external shape of the printed part to remain intact. The proposed approach uses a computational stress analysis to control the distribution of the local density of the infill pattern. We have applied the approach to a wind turbine blade core with infill densities optimized based on the structural loads. The blade core is fabricated in our big area additive manufacturing (BAAM) system. To ensure less warpage and better inter-layer bonding, fast layer deposition is critical in BAAM system. We have optimized the tool path sequences to minimize the deposition time via the solution to the Chinese Postman Problem (CPP). For the application of wind turbine infill, the deposition from the CPP method is twice faster than the deposition from conventional slicing.

1. INTRODUCTION

Extrusion based additive manufacturing is one of the widely used form of 3D printing technologies. It involves the extrusion of polymers and polymer composites through an extruder and depositing the material based on the cross-section shape of a product layer by layer from the

CAMX Conference Proceedings. Dallas, TX, October 15-18, 2018. CAMX – The Composites and Advanced Materials Expo

bottom surface to the top of the product [1, 2]. The cross-section shape of a given layer is obtained via slicing the 3D shape of the product, and slicing software, often called a slicer, defines perimeters, insets, and infill geometry in the 2D cross-section shape of the layer. A perimeter is out-most boundary line of the cross-section, and insets are the inner lines parallel to the perimeter that enclose the infill. The infill is the interior structure of the cross-section shape. Slicers available in the market provide various infill patterns and infill densities [3]. Both infill density and the geometric structure of infill pattern affect the mechanical performance. For a tensile test of dog bone specimen, honeycomb shape infill shows higher modulus [4] than any of diamond, eggcrate, or Hilbert shape with the same amount of material. For a given infill shape, a dense infill will obviously show higher stiffness than a coarse infill due to different amounts of material used. For the same amount of material with a given shape (e.g., honeycomb shape), high mechanical performance can be obtained by redistributing infill density – coarse infill for low stress area and dense infill for high stress area. However, most slicers available in the market do not provide the feature for generating non-uniform, graded infill shape. In our previous study [5], we have developed a mathematical approach for generating honeycomb-shape infill with varying hexagon sizes based on a given stress field. The technology was applied to a wing design with small-scale additive manufacturing [5]. This approach differs from topology optimization. The topology optimization changes the external shape of a product whereas the approach presented in this study focuses on the porous infill and remains the external shape of the printed part intact.

In this paper, we apply our technology of generating graded infill to the wind turbine industry. Based on the design of wind turbine blade and its deflection measurements, we perform stress simulation and obtain an internal stress map. Circle packing algorithms are used to generate a honeycomb-shape infill structure with small and dense hexagon patterns in a high-stress area and large and coarse hexagon patterns in a low-stress area. The infill structure is printed in a large-scale 3D printer, also known as Big Area Additive Manufacturing (BAAM) [6], in Manufacturing Demonstration Facility (MDF) at Oak Ridge National Lab (ORNL). One of the challenges in printing such complex geometry in the BAAM system is to reduce layer deposition time. Toolpath optimization technique is implemented via a mathematical algorithm to reduce the time for successful printing. For the use of the printed structure in wind turbine industry, the total weight should be significantly reduced. Therefore, we have developed a foam feedstock material for 3D printing applications in the BAAM system.

Ultimately, this manufacturing workflow presented in this paper allows for a novel methodology across a number of fronts: (1) A novel design for wind turbine blade cores based on simulated stresses, (2) A novel means of manufacturing the turbine blade core via large-scale 3D printing, (3) A novel implementation of foam material in wind turbines via 3D printing process.

2. LOAD ON WIND TURBINE BLADE

The design of the blade model 442SR blade was obtained from XZERES Corp. As shown in Fig. 1, the blade consists of a root, a mid-span blade, and a tip. The total length is 3.5 m and the length of the mid-span blade is 2.8 m. The skin of the mid-span blade encloses a core structure which is fabricated via our BAAM system in MDF at ORNL

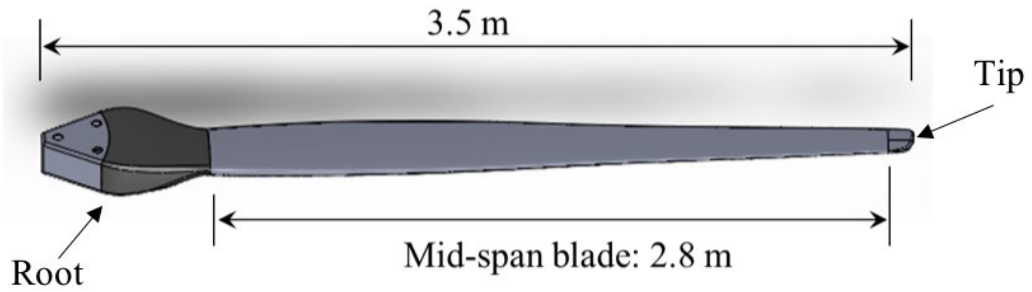

Figure 1. Wind turbine blade with its dimensions

A static test was performed on the Xzeres 442SR blade. The blade was instrumented with string potentiometers placed at 1325, 2530, and 3400mm respectively from the center of rotation of the blade. The deflection data was obtained for the duration of the load test. The deflection was obtained based on the worst case flapwise-direction loading for the blade, and the data show the response of the actual blade to the applied load. The static test and deflection measurements were conducted at Xzeres Wind facility. Shear strain profile was estimated from the second derivative of the deflection, and the deflection of the mid-span blade, shown in Fig. 2(b), was determined from the mid-span blade portion of the shear strain profile.

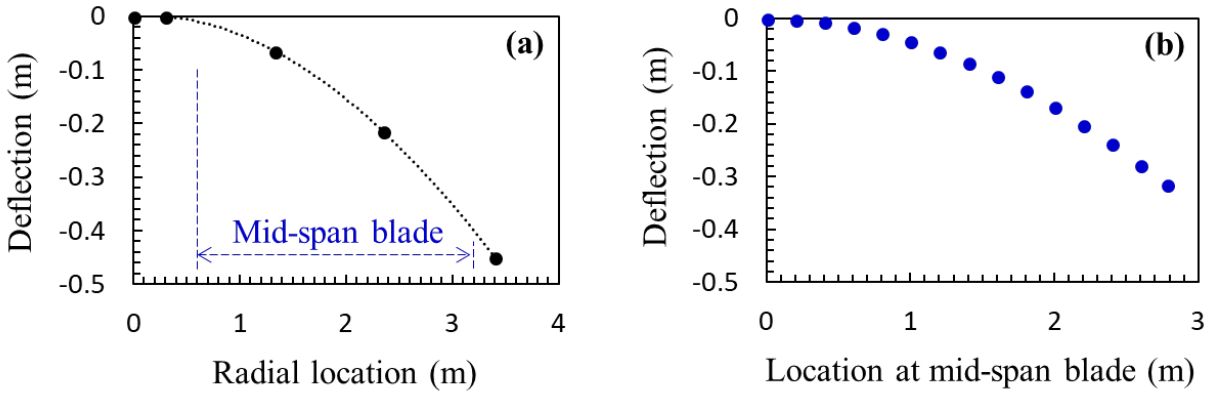

Figure 2. (a) Deflection of the entire blade and (b) Deflection of the mid-span blade

Finite Element Analysis (FEA) was performed on the mid-span blade to obtain a load distribution that matches the deflection profile in Fig. 2(b). A commercial FEA tool, ABAQUS 2017, was used for computational structural analysis. The model is discretized into 110 k tetrahedral elements. To avoid shear locking, the elements use a quadratic interpolation function. The numerical framework utilizes elastic constitutive relations. Figure 3 shows the loading condition and the boundary condition applied in this case. The base surface of the blade is fixed, and a distributed load is applied to the top and bottom surface. The distributed load is in the flapwise-direction of the blade which is indicated as z-direction in Fig. 3.

The load applied to the surface of the mid-span blade was estimated iteratively starting from uniform pressure load and obtaining the deflection from the simulation. A correction factor profile was estimated from the difference between the measured deflection as in Fig. 2(b) and the deflection from the simulation for a given load distribution profile. The load profile was adjusted based on the previous load profile multiplied by the correction factor profile. The adjusted load

was applied to the surface of the blade in the simulation and the corresponding deflection profile is obtained. Figure 4(a) includes deflection profiles from uniform load, linearly varying load, and the adjusted load. The deflection profile from the adjusted load in the simulation closely matches the measured profile in Fig. 2(b). The adjusted load profile is shown in Fig. 4(b).

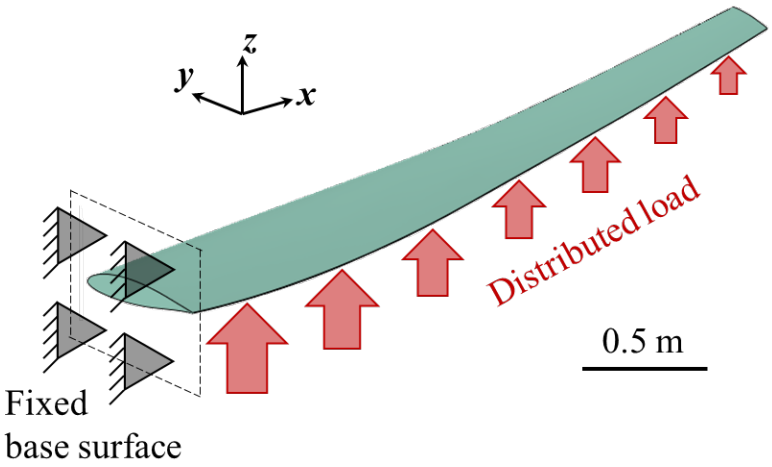

Figure 3. Load and boundary conditions used in FEA

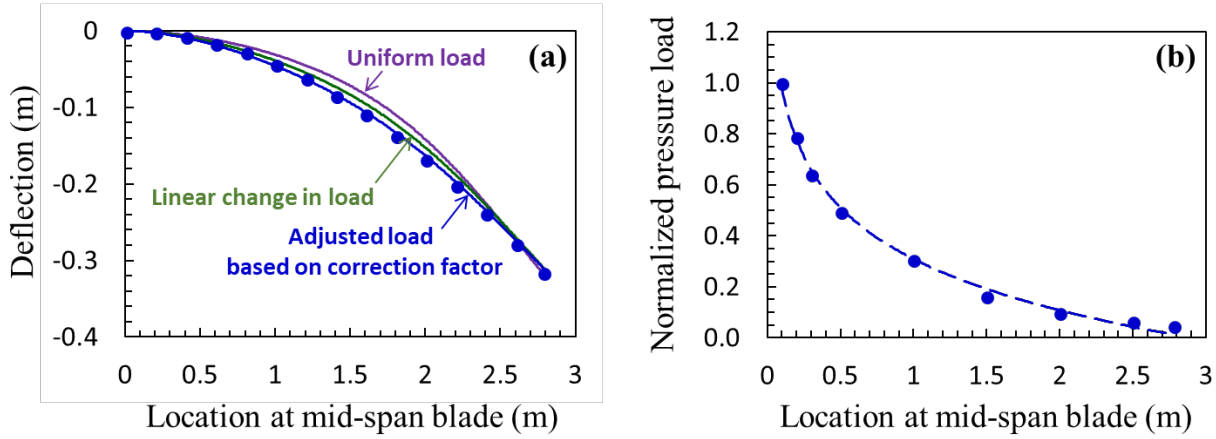

Figure 4. (a) Deflection profiles with various load distributions and (b) Adjusted load distribution

The infill density, which will be discussed in Sec. 3.1, should vary in accordance with the internal stress. the maximum internal stress is generated at the root of the blade and the internal stress gradually decreases as the distance from the blade root increases. The simulation shows that the von Mises stress profile is similar to the hydrostatic pressure profile as shown in Fig. 5. Therefore, the choice of one stress type over another type will not make differences in the infill density optimization.

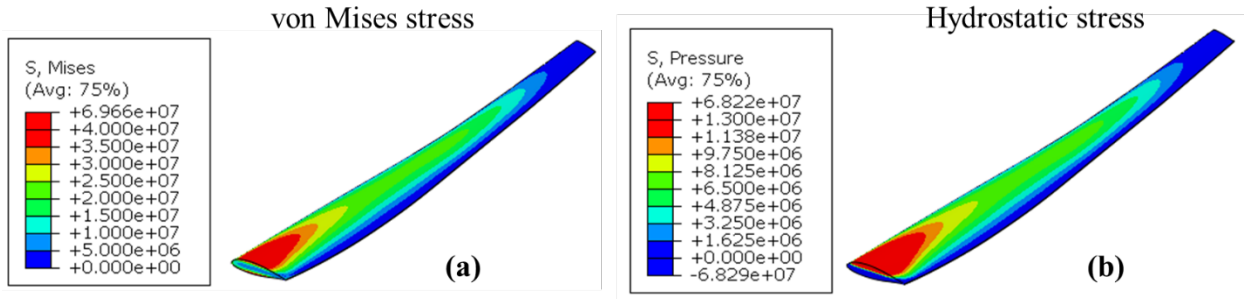

Figure 5. (a) von Mises stress profile and (b) hydrostatic pressure profile

3. OPTIMIZATIONS

3.1 Infill Pattern Optimization via Circle Packing Algorithms

We utilize the method of circle packing generation to create hexagonal infill pattern. This method allows circles to be refined, their centers to be connected via triangulation, a hexagonal mesh to be generated via the dual graph. Two different circle packing algorithms are utilized to generate infill patterns. Stephenson's algorithm [7-10] calculates the unique circle packing that corresponds with a specific set of combinatorics and boundary conditions. Bowers' [11] algorithm calculates a flexible circle packing using relaxed constraints on specific circle tangencies in a force simulation algorithm. The detailed implementation techniques are explained in Ref. [5]. A brief outline of the algorithms is given below.

In Stephenson's method, the packing radii for all circles are determined by maintaining the tangency between circles. In the selected region where the circles should be densely populated, new vertices are inserted by partitioning triangular faces and reconnecting edges. In Bowers' method, a force between neighboring circles is calculated via inverse distance, and a repelling force or a pulling force is applied depending on the overlap or the disjoint between the circles.

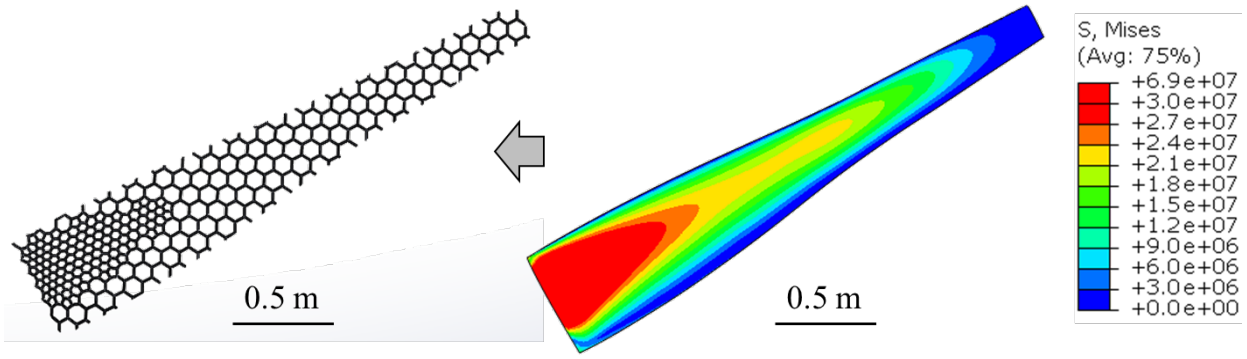

Figure 6. Infill mesh of the blade generated via the circle packing algorithms and the corresponding stress field

Using the two circle packing algorithms, we have generated an infill pattern with a graded honeycomb shape. Figure 6 shows the graded infill geometry and corresponding stress field. Dense and small hexagons are generated in the area with high stress, and sparse and large hexagons are

generated in the area with low stress. The connectivity between hexagons are ensured through the circle packing algorithms and the triangulation. Our earlier study [5] shows that the optimized infill structure shows higher mechanical performance than the uniform infill structure for the same amount of material.

3.2 Toolpath Optimization via Chinese Postman Algorithm (Speeding-Up Algorithm)

3.2.1 Necessity of minimum travel

One of the challenges in printing the honeycomb shape infill in the BAAM system is to reduce layer deposition time. In the previous work in a small scale [5], we used Stratasys Fortus 400 MC with a heated chamber which allows longer layer time with sufficient interlayer bonding strength and minimal warpage. However, in a BAAM system with an open-air build area, our initial attempt to print the infill mesh was not successful, and one of the main reasons is a long layer time (> 30 mins). To reduce the layer deposition time, we have implemented a mathematical algorithm for minimizing total distance of the extruder movement for a given geometry. The algorithm is a solution to the Chinese Postman Problem (CPP) in which a postman needs to go through every street at least one time while minimizing the total travel distance. The mathematical model can be found in Ref. [12-14], and the application to a small-scale 3D printer can be found in Ref. [15].

3.2.2 Chinese postman problem and its implementation in 3D printing

The CPP asks the following question: Having begun at a given vertex on a graph, what is the minimal distance required to traverse all the edges of the graph? A graph $G = (V, E)$ is a vertex set $V = \{v_1, v_2, \dots, v_n\}$, for some integer n, and an edge set $E = \{v_i v_j | i \neq j\}$, where $v_i v_j$ is an edge connecting vertices v_i and v_j and $1 \leq i \leq n$, $1 \leq j \leq n$. For this application, we let $v_i = (x_i, y_i)$, points to be traversed by a 3D printer's extruder, but theoretically v_i can be any element in a set. The degree of a vertex is the number of neighboring vertices to a given vertex. For instance, if vertex v_1 is connected to vertex v_{25} by an edge, to v_{174} by an edge, to vertex $v_3$by an edge, and to vertex v_7 by an edge, then vertex v_1 has degree four. If a vertex has odd degree, we call it an odd vertex, and likewise for even vertices. An ordered list of the degrees of all the vertices of a graph is called the graph's degree sequence.

To solve the CPP for a given graph is equivalent to find all Eulerian cycles from a given vertex on a graph. A cycle is a sequence of edges in a graph that ends where it begins. A graph is called Eulerian graph if it can be drawn without picking up a pen. If, in attempting to find the Eulerian cycles that start at a given vertex in a graph, there are paths that are not Eulerian cycles, then one can add edges to the graph to make those incomplete paths Eulerian. The key to an appropriate algorithm for solving the CPP is therefore equivalent to finding Eulerian cycles from a starting vertex or completing Eulerian cycles by adding edges to the graph in some optimal way. This process is equivalent to, in a pure graph theoretic sense, backtracking in the shortest path possible along previously visited edges.

For 3D printing, we are not constrained to the edges of the graph, one can move the printhead along the added edges by ceasing the extrusion, lifting the extruder from the print, and moving the extruder to another location in the air. By eliminating such constraint, optimization of the process involves searching those vertices that break Eulerian cycles and match them such that the distance between matched vertices is minimized.

3.2.3 Improvement of the deposition time in BAAM

The innovative toolpath optimization allows for layer time to be decreased. We generated a gcode for two layers as a test case from the optimized toolpath via Chinese postman algorithm, and printed the infill pattern with Acrylonitrile Butadiene Styrene (ABS) with 20% by weight Carbon Fiber (CF) composites as shown in Fig. 7. For the same infill structure, we have also printed with a toolpath directly from the current version of ORNL slicer (as of May 2018) without toolpath optimization and compare the deposition time between non-optimized toolpath and optimized toolpath via Chinese postman algorithm. As shown in Table 1, printing with toolpath optimization reduces the deposition time by half as compared to printing with non-optimized toolpath.

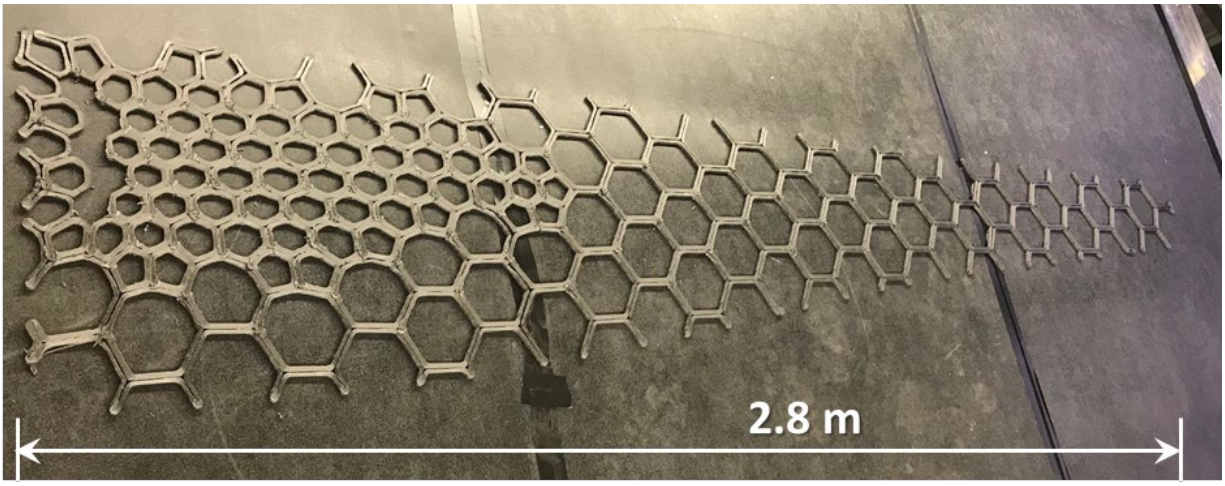

Figure 7. 3D printed infill pattern of wind turbine blade in BAAM. For comparison purposes, only small number of layers (2 layers) are printed. Both optimized toolpath and non-optimized toolpath have the same infill shape.

Table 1. Comparison of the deposition time between optimized and non-optimized toolpath

	Optimized Toolpath via Chinese Postman	Non-Optimized Toolpath from current ORNL Slicer
Deposition Time	16 min 5 sec	33 min 6 sec

4. FABRICATION OF AN INFILL VIA BAAM

We have printed the infill of the mid span blade in the BAAM system with aforementioned processes including circle packing algorithm and toolpath optimization. Figure 8(a) shows the print with ABS/CF 20% by weight composites.

One of the requirements for a wind turbine blade is its light-weight. The material of ABS/CF20%wt. has relatively high density (i.e., 1.14 g/cc) which is not suitable for wind blade core application. We have recently developed foam formulations for BAAM feedstock material. Figure 8(b) shows a printed hexagon using one of the developed foam materials. The material is a thermoplastic polyurethanes (TPUs) with a foaming agent. The density of the foam varies between 0.25 g/cc and 0.3 g/cc depending on the printing conditions.

By switching the material from ABS/CF to foam, multiple printing conditions should be modified and carefully calibrated including temperature profiles, screw rotational speed, and extrusion throughput. Moreover, the foam material has a much lower viscosity and it requires a limited resident time in the barrel to avoid cooking. A change of these parameters affects the print quality and the mechanical performances of the final printed structure. We have successfully printed a few layers of the blade infill as shown in Fig. 8(c). More calibrations and optimizations of the printing parameters are being planned and tested.

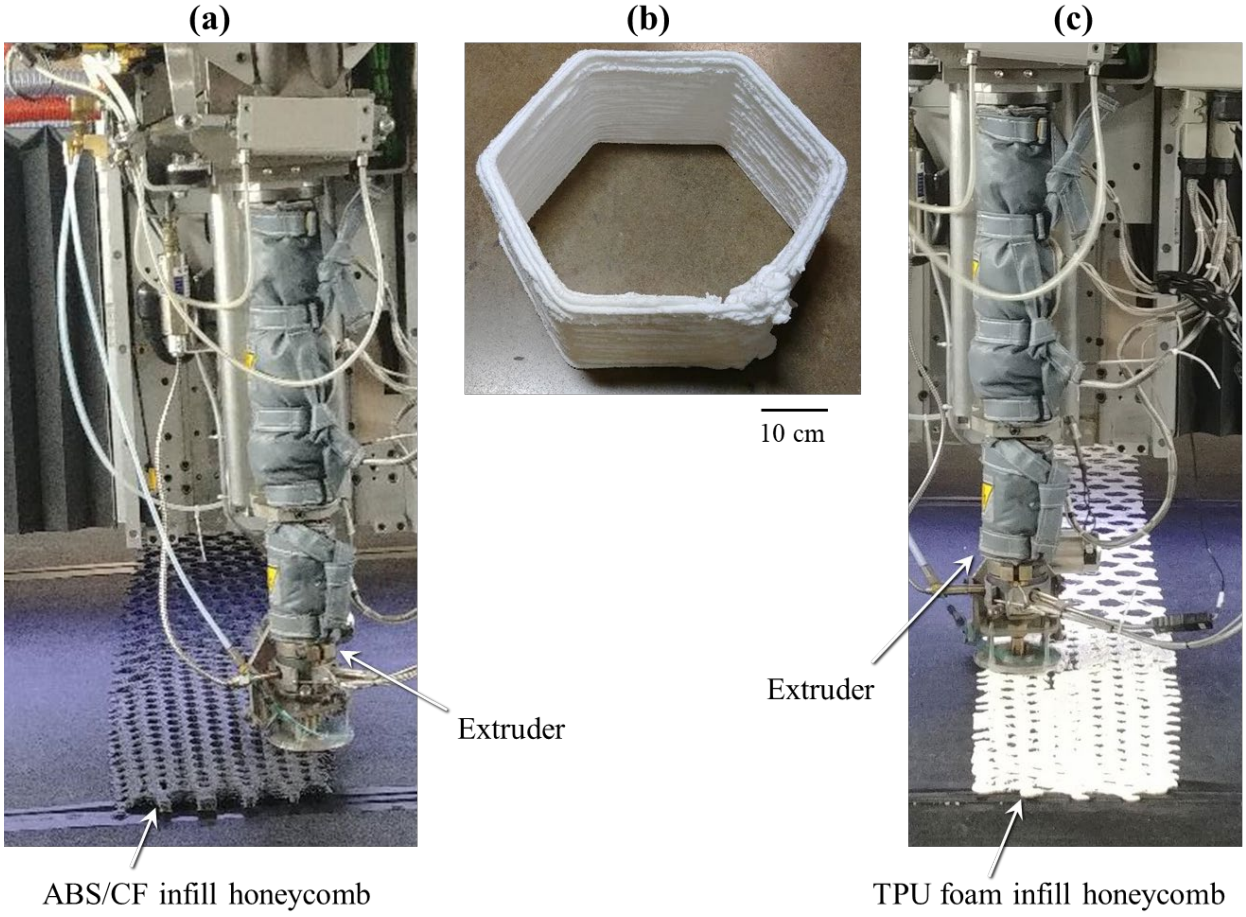

Figure 8. (a) Blade infill printed with ABS/CF 20%wt., (b) Foam material developed for BAAM applications, and (c) Three layers of test printing of blade infill with foam

5. CONCLUSIONS

We have developed an approach to generate graded infill structure for wind turbine applications. The deflection of a wind turbine blade from Xzeres Corp. was measured, and the stress was analyzed via finite element simulation. To generate an optimal infill structure, the distribution of the local density of the honeycomb infill pattern was controlled based on the stress field from the simulation. Specifically, circle packing algorithms were used to generate the graded infill structure in which small circles are densely packed for high stress areas. The generated infill structure was printed using the big area additive manufacturing (BAAM) system. To reduce the layer deposition time, we have optimized the toolpath by implementing a mathematical algorithm for minimizing total distance of the extruder movement. The algorithm is a solution to the Chinese postman problem. The result of the implementation shows that the deposition time is reduced by half after the toolpath optimization.

Initial print with carbon fiber-reinforced ABS composite was successful. However, the material is not suitable for the core of wind turbine blade because of its high density. We have developed a low-density thermoplastic polyurethane based foam material to replace the conventional ABS/CF composite. For successful printing in BAAM with foam, calibrations of the printing parameters are being planned.

ACKNOWLEDGEMENTS

Research sponsored by the U.S. Department of Energy, Office of Energy Efficiency and Renewable Energy, Industrial Technologies Program, under contract DE-AC05-00OR22725 with UT-Battelle, LLC.

6. REFERENCES

1. S. Mellor, L. Hao and D. Zhang, *Additive manufacturing: A framework for implementation.* International Journal of Production Economics, 2014. **149**: p. 194-201.
2. W. Gao, Y. Zhang, D. Ramanujan, et al., *The status, challenges, and future of additive manufacturing in engineering.* Computer-Aided Design, 2015. **69**: p. 65-89.
3. *Slic3r Infill Patterns*. Available from: http://manual.slic3r.org/expert-mode/infill.
4. D. Adams and C.J. Turner, *An implicit slicing method for additive manufacturing processes.* Virtual and Physical Prototyping, 2018. **13**(1): p. 2-7.
5. S. Kim, X. Chen, G. Dreifus, et al., *An integrated design approach for infill patterning of fused deposition modeling and its application to an airfoil*, in *SAMPE*. 2017: Seattle, WA.
6. L.J. Love, C.E. Duty, B.K. Post, R.F. Lind, P.D. Lloyd, and V. Kunc, *Breaking Barriers in Polymer Additive Manufacturing*. 2015, Manufacturing Demonstration Facility at Oak Ridge National Lab: Conference: SAMPE, Baltimore, MD.
7. G. Dreifus, K. Goodrick, S. Giles, et al., *Path Optimization Along Lattices in Additive Manufacturing Using the Chinese Postman Problem.* 3D Printing and Additive Manufacturing, 2017. **4**(2): p. 98-104.
8. C.R. Collins and K. Stephenson, *A circle packing algorithm.* Computational Geometry, 2003. **25**(3): p. 233-256.

9. K. Stephenson, *Circle packing: a mathematical tale.* Notices of the AMS, 2003. **50**(11): p. 1376-1388.
10. G. Dreifus, B. Rapone, X. Chen, J. Bowers, B. Braswell, and B. Krishnamoorthy. *A new approach to tool path generation in additive manufacturing, in Symposium on Computational Fabrication*. in *Symposium on Computational Fabrication*. 2017.
11. J.C. Bowers and P.L. Bowers, *Ma–Schlenker c-Octahedra in the 2-Sphere.* Discrete & Computational Geometry, 2018. **60**(1): p. 9-26.
12. R. Dwivedi and R. Kovacevic, *Automated torch path planning using polygon subdivision for solid freeform fabrication based on welding.* Journal of Manufacturing Systems, 2004. **23**(4): p. 278-291.
13. D. Jungnickel, *Chapter 2. Algorithms and Complexity*, in *Graphs, Networks and Algorithms*. 2013, Springer.
14. P. Bollweg, D. Hasanbegovic, H. Müller, and M. Stöneberg, *Surface-adaptive and Collision-avoiding Path Planning for Five-axis Milling*. 2006, Department of Informatics, TU Dortmund.
15. G. Dreifus, K.J. Goodrick, S.M. Giles, et al. *Path Optimization Along Lattices in Additive Manufacturing Using the Chinese Postman Problem*. in *3D Printing and Additive Manufacturing*. 2017.